Using the Inverse Method to Estimate the Solar Absorptivity and Emissivity of Wood Exposed to the Outdoor Environment

Kang, Wook
Department of Wood Science and Engineering, Division of Forest Resources & Landscape Architecture, Chonnam National University

Lee, Yong-Hun
Department of Mathematics, and Institute of Pure and Applied Mathematics, Chonbuk National University

Kang, Chun-Won
Department of Housing environmental design, and research institute of human ecology, College of Human Ecology, Chonbuk National University

Chung, Woo-Yang
Department of Wood Science and Engineering, Division of Forest Resources & Landscape Architecture, Chonnam National University

他

https://doi.org/10.5109/19542

出版情報：九州大学大学院農学研究院紀要. 56 (1), pp.139-148, 2011-02. 九州大学大学院農学研究院
バージョン：
権利関係：

J. Fac. Agr., Kyushu Univ., **56** (1), 139–148 (2011)

Using the Inverse Method to Estimate the Solar Absorptivity and Emissivity of Wood Exposed to the Outdoor Environment

Wook KANG[1], Yong–Hun LEE[2], Chun–Won KANG[3]*, Woo–Yang CHUNG[1], Hui–Lan XU[1] and Junji MATSUMURA[4]

Laboratory of Wood Science, Division of Sustainable Bioresources Science,
Department of Agro–environmental Sciences, Faculty of Agriculture,
Kyushu University, Fukuoka 812–8581, Japan
(*Received October 28, 2010 and accepted November 8, 2010*)

This study used the inverse method to investigate the solar absorptivity and emissivity of wood. The solar absorptivity and emissivity estimates were 0.396 (0.308~0.570) and 0.526 (0.307~0.772), respectively. They were highly dependent on the boundary conditions of convective heat transfer coefficients. Emissivity was much lower than that seen in most previous studies. Absorptivity was closely related to the L*a*b* color system, mainly to whiteness. It increased with increasing density because lightness or whiteness has the highest correlation with density. There was a weak positive correlation between absorptivity and emissivity overall with R^2=0.223.

Keywords: heat transfer, inverse method, solar absorptivity, wood color, solar emissivity, solar radiation

INTRODUCTION

Knowledge of the thermal behavior of wood exposed to the outdoors is important for assessing the durability and expected performance of any exterior wooden component. The degradation of exterior wood is closely related to diurnal and seasonal temperature variations. Furthermore, thermal behavior also affects moisture transfer, and, hence, plays an important role in determining the moisture gradient in wood. The thermal performance of exterior wood depends on the outdoor environment, as well as on intrinsic material properties. Stresses encountered in the outdoor environment include the effects of solar radiation, wind velocity, air temperature, and relative humidity. Material properties include solar absorptivity and longwave emissivity.

Heyer (1963) reported that the temperatures in walls and roofs could rise appreciably above the ambient air temperature, based on data from six residential houses and one office building. The maximum values in walls and roof can occasionally exceed 54 and 77 ˚C. The surface temperature on wood may rise more than 20 ˚C higher than the ambient air temperature during the daytime (Shida *et al*., 1991). During the night, however, the surface temperature of the wood may be as much as 5~8 ˚C colder than the ambient outdoor air, as a result of heat loss via radiation to the sky (Tenwolde, 1997).

Diurnal temperature variation in wood is influenced by the radiant solar energy absorptivity and emissivity in any given outdoor environment. In the field of wood physics, Wengert (1965) first predicted the maximum surface temperature of wood exposed to exterior conditions. He adopted a simplified energy balance equation that did not consider heat conduction. Shida *et al*. (1991) measured the daily variation in surface temperatures of a wooden deck. Computer models have been developed that predict the temperature of roof sheathing and other roof structures (Tenwolde, 1997, Wilkes, 1989). To simulate the roof surface temperature, Tenwolde (1997) adopted 0.65 and 0.90 as the values of absorptivity and emissivity of shingles, respectively. However, the model consistently overestimates night–time cooling from sky radiation losses, leading to predicted temperatures that are too low. He explained that the discrepancy might be due to the heat gain from nocturnal radiation from surrounding buildings and other objects, or possibly due to having adopted too high a value for emissivity.

The surface color of a material is an important factor affecting its thermal performance and is closely related to solar absorptivity and reflectivity. The absorptivity is smaller for materials having a smooth and light–colored surface, while it is greater for those having a rough and dark–colored surface. Bansal *et al*. (1992) studied the effect of exterior surface color on the thermal performance of buildings. They found that enclosures painted black recorded a maximum of 7 ˚C higher temperatures than the corresponding white ones during the hours of maximum solar radiation. During the night, the two enclosures had nearly the same temperatures. Therefore, absorptivity may also change depending on the wood species, because the color of wood differs widely among species (Nishino *et al*., 1998).

[1] Department of Wood Science and Engineering, Division of Forest Resources & Landscape Architecture, Chonnam National University, Gwangju 500–757, Republic of Korea
[2] Department of Mathematics, and Institute of Pure and Applied Mathematics, Chonbuk National University, Jeonju 561–756, Republic of Korea
[3] Department of Housing environmental design, and research institute of human ecology, College of Human Ecology, Chonbuk National University, Jeonju 561–756, Republic of Korea
[4] Laboratory of Wood Science, Division of Sustainable Bioresources Science, Department of Agro–environmental Sciences, Faculty of Agriculture, Kyushu University, Fukuoka 812–8581, Japan
* Corresponding author (E–mail: kcwon@jbnu.ac.kr)

However, there are few studies available on the solar absorptivity and longwave emissivity of wood species because direct measurement on the broadband frequency range is difficult, especially in case of emissivity. Therefore, this study was conducted to estimate solar absorptivity and longwave emissivity indirectly using the inverse method after measuring the surface temperature of Korean wood and tropical hardwood horizontally exposed to an outdoor environment. The effects of surface color and density on the absorptivity and emissivity were also investigated.

MATERIALS AND METHODS

Measurements of color and temperature

Ninety–seven wood species, fifty–one species of Korean wood and forty–six species of tropical hardwood were used to measure the color and the surface temperature (Tables 1 and 2). All of the specimens were wood identification samples with flat grain and were resurfaced with 120 mesh abrasive paper. The dimensions of the specimens were approximately 140mm×70mm×10mm. The specimens were measured with a colorimeter (Minolta CR–10) to obtain the colorimetric values of L*, a*, and b*. In order to eliminate radiative heat transfer from the ground, five of the surfaces were insulated with polystyrene foam boards, leaving only the top surface exposed. Field tests were undertaken to measure the horizontal surface temperature of the wood and at Chonnam National University in Gwangju, Korea, on two clear days – the 30th of April and the 5th of June 2009. The surface temperature was measured with K–type thermocouples centered on the specimen and covered with aluminum tape to minimize measurement error. Using a data logger with 67 channels, instantaneous temperature readings of the surface of the wood were taken every minute for a period of twenty–four hours. At a nearby weather station we collected data on ambient temperature, relative humidity, wind speed, and incident solar radiation at one minute intervals (Davis Instruments, Weatherlink Vantage Pro2).

A heat transfer model for solar radiation

The one–dimensional heat transfer equation can be expressed by

$$\rho C_p \frac{\partial T}{\partial t} = \frac{\partial}{\partial x}\left(k \frac{\partial T}{\partial x}\right) \quad (1)$$

where T : temperature (K)
ρ : wood density (kg/m^3)
k : thermal conductivity (W/m K)
C_p : heat capacity (J/kg K)

The boundary conditions are given by

$$-k \frac{\partial T}{\partial x} = 0 \quad \text{at x = 0} \quad (2)$$

$$-k \frac{\partial T}{\partial x} = \overline{h_{nc} + h_{fc}} \, (T_s - T_a) - q_{r,net} \quad \text{at x = } l \quad (3)$$

where $q_{r,net}$: net radiance at the surface of the wood (W/m^2)
h_{nc} : natural convective heat transfer coefficient (W/m^2 K),
h_{fc} : forced convective heat transfer coefficient (W/m^2 K),
T_s : temperature on the surface of the wood (K)
T_a : air temperature (K)

The natural and convective heat transfer equation adopted from Wilkes (1989) and Tenwolde (1997) is dimensionless.

The approximate thermal conductivity and heat capacity are predicted from The Wood Handbook (1999).

$$k = 0.01864 + \rho_0 (0.1941 + 0.4064m) \quad (4)$$

$$C_p = \frac{103.1 + 3.867T + 4190m}{1 + m} + m(-6191 + 23.6T - 1330m) \quad (5)$$

ρ_0 : dry wood density (g/cm^3)
m : moisture content (kg/kg)

The combined convective heat transfer coefficient, which includes natural and forced transfer was also adopted from Wilkes (1989) and Tenwolde (1997).

The general solar radiation balance may be written as

$$q_{r,net} = \alpha G - \varepsilon \Delta R \quad (6)$$

α : solar absorptivity (–)
G : incident solar radiance (W/m^2)
ε : longwave emissivity of the surface (–)
ΔR : difference between longwave radiation incident on the surface from the sky, surroundings and black–body radiation emitted at ambient outdoor air temperature (W/m^2)

Emissivity is defined as the ratio of surface radiation to black–body radiation at the same temperature. Any solid surface, such as wood, emits energy away from itself, the intensity of which is dependent on the temperature of the solid. The emitted energy can be expressed as $\varepsilon \sigma T_s^4$. Energy from surrounding objects, on the other hand, is absorbed by the solid surface. If L is the incident long–wave radiation, then the absorbed energy is εL. Therefore, Eq. (6) can be expressed as follows (Kragh MK, 1998),

$$q_{r,net} = \alpha G + \varepsilon L - \varepsilon \sigma T_s^4 \quad (7)$$

L : the incident long–wave radiance (W/m^2)
σ : the Stefan–Boltzmann constant (5.67×10^{-8} W/m^2 K^4)
T_s : the surface temperature (K)

Table 1. Color and thermophysical properties of the Korean wood specimens

Species		Common name	Density (kg/m^3)	Colorimetric values			Solar properties	
Scientific name				L	a	b	α	ε
Softwood								
Abies holophylla		Needle fir	436	72.0	10.7	24.9	0.393	0.600
Abies koreana		Korean fir	347	77.9	8.50	22.8	0.342	0.632
Abies nephrolepis		Khingan fir	336	76.0	9.20	24.4	0.365	0.619
Ginkgo biloba		Maidenhair tree	523	70.6	10.8	24.7	0.308	0.410
Larix leptolepis		Japanese larch	546	48.7	16.3	21.2	0.444	0.522
Picea jezoensis		Yezo spruce	394	70.9	10.3	23.0	0.371	0.497
Picea koraiensis		Korean spruce	498	73.6	9.70	24.0	0.358	0.534
Pinus Banksiana		Jack pine	477	76.4	9.00	23.2	0.351	0.444
Pinus densiflora		Japanese red pine	508	69.6	10.8	24.2	0.430	0.662
Pinus parviflora		Japanese white pine	429	71.8	10.0	23.0	0.318	0.431
Pinus rigida		Pitch pine	560	75.0	8.80	21.8	0.319	0.427
Pinus strobus		White pine	367	76.2	8.50	21.0	0.339	0.364
Tbuja orientalis		Chinese arborvitae	385	63.3	9.30	20.2	0.431	0.561
Tsuga sieboldii		Japanese hemlock	637	69.3	9.80	23.0	0.392	0.527
Hardwood								
Ailantbus altissima		Tree of heaven	644	77.4	7.90	22.7	0.394	0.692
Alnus birsuta var. sibirica		Siberian alder	561	69.3	10.9	19.5	0.404	0.658
Alnus japonica		Japanese alder	499	67.5	10.6	20.0	0.399	0.627
Betula costata Trautretter		Costata birch	662	75.1	9.80	20.8	0.336	0.577
Betula platypbylla Sukatchev var. japonica		White birch	535	75.5	9.10	20.5	0.329	0.534
Carpinus laxiflora		Horn beam	713	73.8	7.80	21.0	0.369	0.494
Castanea crenata		Japanese chestnut	621	58.5	11.5	23.4	0.411	0.651
Cedrela sinensis		Chinese cedrela	634	49.6	17.6	21.1	0.453	0.656
Celtis sinensis		Japanese hackberry	698	80.1	8.20	23.1	0.354	0.531
Cornus controversa		Giant dogwood	550	69.3	9.80	25.0	0.346	0.542
Cornus Walteri		Korean dogwood	802	62.3	13.6	21.3	0.388	0.532
Evodia Daniellii		Korean Evodia	628	71.5	7.70	19.7	0.407	0.615
Fraxinus mandsburica		manchurian ash	694	68.5	8.40	20.7	0.427	0.620
Fraxinus rbyncbopbylla		Korean ash	656	73.1	8.30	23.7	0.472	0.752
Hemiptelea Davidii		David hemiptelea	685	66.8	12.3	22.2	0.414	0.711
Hovenia dulcis		Japanese raisin tree	579	62.4	13.6	21.5	0.340	0.448
Juglans mandsburica		Mandscurica walnut	520	69.9	10.0	20.0	0.373	0.522
Kalopanax pictus		Castor aralia	585	73.7	9.50	24.3	0.308	0.432
Maackia amurensis		Amur maackia	554	47.7	12.0	18.1	0.461	0.440
Melia Azedarach var. japonica		Japanese bead tree	430	68.8	12.0	22.2	0.353	0.622
Prunus Padus		Bird cherry	593	64.1	11.4	20.5	0.314	0.401
Quercus acuta		Japanese evergreen oak	888	61.2	13.4	22.4	0.426	0.658
Quercus aliena		Oriental white oak	750	61.6	10.8	22.5	0.443	0.712
Quercus dentate		Daimyo oak	843	62.6	11.6	22.2	0.355	0.480
Quercus serrata		Konara oak	760	68.4	9.20	24.3	0.400	0.627
Quercus Tscbonoskii var. eximia		Mongolian oak	747	63.2	9.70	21.3	0.494	0.772
Robinia Pseudo–Acacia		Black locust	810	64.8	13.1	25.6	0.460	0.745
Salix koreensis		Korean willow	547	73.4	9.30	18.7	0.350	0.590
Sorbus alnifolia		Korean mountain ash	612	64.3	11.5	20.0	0.419	0.612
Styrax japonica		Japanese snowbell	588	78.5	8.50	22.2	0.320	0.564
Tilia amurensis		Amur linden	388	70.7	9.90	19.5	0.315	0.440
Tilia mandsburica		Manchurian linden	390	73.3	9.30	19.3	0.328	0.459
Ulmus laciniata		Manchurian	709	67.9	11.2	21.7	0.396	0.520
Ulmus parvifolia		Chinese elm	738	65.5	10.5	19.8	0.394	0.582
Ulmus pumila		Siberian elm	638	70.6	10.0	23.0	0.353	0.403
Ulnus Davidiana var. japonica		Japanese elm	643	63.4	9.80	19.5	0.407	0.598
Zelkova serrata		Zelkova	751	62.4	13.4	21.3	0.399	0.709

Table 2. Color and thermophysical properties of the tropical hardwoods

Species	Common name	Density (kg/m^3)	Colorimetiric values			Solar properties	
Scientific name			L	a	b	α	ε
Alstonia angustiloba	Pulai	472	72.1	7.00	19.7	0.374	0.454
Anisoptera spp.	Mersawa	590	59.8	12.1	23.3	0.456	0.497
Artocarpus spp	Terap	537	48.3	15.7	23.1	0.457	0.516
Artocarpus spp.	Keledang	638	42.4	11.8	15.1	0.457	0.498
Burseraceae spp.	kedondong	499	65.6	10.3	18.3	0.356	0.365
Carallia spp	Meransi	764	58.3	15.3	23.2	0.415	0.535
Cotylelobium spp.	Resak	776	46.3	9.90	14.2	0.498	0.504
Cratoxylon arborescens	Geronggang	542	54.0	15.4	19.3	0.428	0.600
Cynometra ripa	Kekatong	1068	54.6	10.2	15.2	0.474	0.460
Dialium spp.	Keranji	1181	41.7	13.3	13.9	0.570	0.703
Dillenia spp.	Simpoh	740	53.0	12.3	13.3	0.449	0.520
Dipterocarpus spp.	Keruing	1016	51.4	11.7	14.1	0.461	0.469
Dyera costulata	Jelutong	409	76.5	9.70	28.3	0.308	0.424
Endospermum spp.	Sesendok	544	71.5	8.90	22.4	0.345	0.412
Eugenia spp.	Kelat	864	52.4	10.3	15.7	0.438	0.389
Fagraea fragrans	Tembusu	908	63.0	10.5	19.6	0.464	0.643
Gonystylus spp.	Ramin	662	72.9	10.9	27.9	0.338	0.390
Heritiera spp	Mengkulang	523	62.9	8.20	15.5	0.397	0.490
Hevea brasiliensis	Rubberwood	667	71.9	8.70	20.1	0.337	0.452
Hopea spp.	Merawan	549	56.5	13.9	25.6	0.394	0.466
Intsia spp.	Merbau	924	42.1	14.2	13.3	0.540	0.687
Koompassia malaccensis	Kempas	816	55.3	14.5	19.0	0.415	0.440
Lauraceae spp.	Medang	520	51.8	12.9	19.5	0.403	0.481
Lophopetalum	Perupok	516	70.4	8.10	17.4	0.357	0.565
Madhuca utilis	Bitis	1108	41.7	12.4	11.9	0.507	0.629
Mangifera spp.	Machang	597	68.4	8.70	18.0	0.382	0.517
Neobalanocarpus heimii	Cengal	841	41.1	13.8	15.0	0.406	0.516
Parashorea spp.	Gerutu	785	59.5	11.2	21.2	0.444	0.578
Parishia spp.	Sepul	475	68.5	7.70	17.0	0.355	0.475
Parkia spp.	Petai	414	74.1	7.70	20.6	0.334	0.471
Pentace spp	Melunak	842	49.3	13.2	15.9	0.447	0.494
Pithecellobium spp.	Kungkur	599	54.4	12.0	20.0	0.370	0.422
Podocarpus spp	Podo	535	62.1	9.20	19.0	0.349	0.387
Pomestia spp.	Kasai	794	52.9	11.0	13.8	0.399	0.361
Sapotaceae spp.	Nyatoh	883	55.6	11.9	16.4	0.430	0.472
Scaphium spp.	Kembang semangkok	682	71.5	9.00	21.8	0.361	0.538
Scorodocarpus borneensis	Kulim	986	45.0	10.5	12.2	0.460	0.460
Shorea acuminate	Dark red meranti	685	58.3	10.9	18.3	0.385	0.378
Shorea assamica Philippinensis	White meranti	684	64.8	11.6	23.6	0.397	0.572
Shorea balangeran	Balau	1047	54.7	12.0	18.6	0.502	0.526
Shorea faguetiana	Yellow meranti	622	62.6	9.50	22.2	0.381	0.462
Shorea leprosula	Light red meranti	521	65.0	9.30	21.3	0.360	0.401
Shorea macroptera	Melantai	476	66.5	9.20	20.6	0.356	0.538
Shorea uliginosa	Meranti bakau	661	52.7	13.1	19.4	0.410	0.307
Sindora spp.	Sepetir	690	61.7	11.5	18.2	0.382	0.429
Swintonia spp.	Merpauh	727	60.4	10.2	18.3	0.341	0.365
Tetramerista glabra	Punah	694	66.7	11.9	23.1	0.397	0.487

Cole (1976a, 1979) carried out a study on incident long–wave radiance on the external surfaces of buildings. He proposed a set of equations following for the calculation of incident long–wave radiance on the basis of ambient dry–bulb temperature and cloud cover.

$$L = 222+4.94(T_a - 273.15)+[65+1.39(T_a - 273.15)]c \quad (8)$$

L : the incident long–wave radiance upon the horizontal surface (W/m^2)
T_a : the ambient dry–bulb temperature (K)
c : the fractional cloud cover (–)

Assuming $L = \sigma T^4_{sky}$ for the horizontal surface, therefore, the net radiance can be expressed by the following equation (Duffie and Beckman, 1991)

$$q_{r,net} = \alpha G - \varepsilon\sigma\,(T_s^4 - T_{sky}^4) \tag{9}$$

T_{sky}(K) is the equivalent blackbody sky temperature, defined to be the equivalent temperature of the clouds, water vapor, and other atmospheric elements that make up the sky to which a surface can radiate heat. Sky temperature is an important parameter for calculating radiative heat transfer between an object at a given temperature above absolute zero (0 K) and the sky.

The fictive sky temperature depends on the exterior air temperature, humidity, and cloudiness. For a partially overcast sky it may be estimated by the equation by Cole (1976b).

$$T_{sky} = T_a[\,\varepsilon_0 + 0.84c(1-\varepsilon_0)]^{0.25} \tag{10}$$

ε_0 : emissivity of the clear sky(–)
c : the fractional cloud cover (–)

Berdahl and Martin (1984) proposed an equation for the emissivity of a clear sky depending on the dew point and time in relation to midnight.

$$\varepsilon_0 = 0.711 + 0.0056t_{dp} + 0.000073t_{dp}^2 + 0.013\cos\left(2\pi\frac{n}{24}\right) \tag{11}$$

t_{dp} : the ambient dew point (°C)
n : time until or since midnight in hours ($0 \le n \le 24$)

For dew points between –20 °C and 30 °C, this equation is valid only for clear sky conditions. The difference between air and sky temperature is from 5 K in a hot and moist climate to 30 K in a cold and dry climate.

$$p_{vs} = \exp[23.5771 - 4042.9/(T_a - 37.58)] \tag{12}$$

$$p_v = P_{vs} \times \phi \tag{13}$$

$$T_{dp} = 37.58 - \frac{4042.9}{\log(p_v) - 23.5771} \tag{14}$$

p_{vs} : saturated water vapor pressure (Pa)
p_v : water vapor pressure (Pa)
T_{dp} : dew point (K)
ϕ : relative humidity (–)

Numerical methods

In this section, we introduce the control volume finite element method (CVFEM) and the Gauss–Newton method, which are used to discretize the heat transfer equation, Eq. (1), and estimate the minimizers of the given functional, respectively.

Control volume finite element method

Consider the one–dimensional heat transfer equation defined by Eq. (1) with two point boundary conditions. In order to find the computational solution of the heat transfer equation, we apply the control volume finite element method which is appropriate for the representation of the flow.

First, we take some mesh

$$\Pi = \left\{(x_i, t_j)\,|\,0 = t_0 < t_1 < \ldots < t_n,\ 0 = x_0 < x_1 < \ldots < x_m = l\right\} \tag{15}$$

and at each node x_i, construct a corresponding control volume, as depicted in Figure 1.

Applying a time discretization technique, such as the backward Euler or the Crank–Nicolson scheme to Eq. (15), we have the following stationary equation at each time step

$$\rho C_p \frac{T - T^{(prev)}}{\Delta t} - \frac{\partial}{\partial x}\left(k\frac{\partial T}{\partial x}\right) = 0 \tag{16}$$

where $T^{(prev)}$ means the value of the temperature at the previous time step and Δt means the time step size. To obtain the discretized formulation of the stationary Eq. (16), we have integrated each control volume, interval [E, W] (see Figure 1) and using the Gauss–divergence theorem, we have the following discrete form

$$\rho C_p \frac{Area(CV)}{\Delta t^j}\,(T_i^{j+1} - T_i^j) = \sum_{f=E,W}\left[k^{j+1}\frac{\partial T^{j+1}}{\partial x}\right]\cdot n_f \tag{17}$$

where superscript (j) and subscript (i) represent the time layer and the nodes, respectively and n_f means the outward normal vector at each end point of the control volume. Area (CV) is the area of the control volume or, in this case, the length of the interval.

At end points E and W, the value of the k^{j+1} is given by the average value, as follows:

$$k^{j+1}\big|_W = (k_i^{j+1} - k_{i+1}^{j+1})/2$$
$$k^{j+1}\big|_E = (k_{i-1}^{j+1} - k_i^{j+1})/2 \tag{18}$$

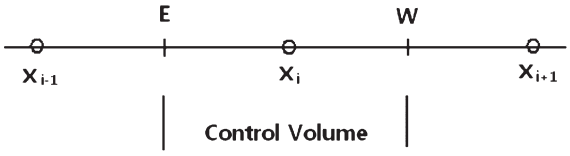

Fig. 1. Nodes and control volume.

and the derivative is approximated numerically

$$\left.\frac{\partial T^{j+1}}{\partial x}\right|_W = \frac{T_{i+1}^{j+1} - T_i^{j+1}}{x_{i+1} - x_i}$$
$$\left.\frac{\partial T^{j+1}}{\partial x}\right|_E = \frac{T_i^{j+1} - T_{i-1}^{j+1}}{x_i - x_{i-1}} \tag{19}$$

At the *(j+1)*–th time, the values $T^{(j)}$ at the *(j)*–th time are known. Hence, as shown in Eq. (17), each

equation can be obtained T_{i-1}^{j+1}, T_i^{j+1}, and T_{i+1}^{j+1}. However, the system of equations must be non–linear. Thus, we use an iterative method, such as Newton's iteration.

Least–Squares method, Gauss–Newton method

If the values of the coefficients and boundary conditions are given, then we can find the computational solution of a boundary value problem of a heat transfer equation. However, we do not have the exact data of some characteristic values of the material and of nature. So, by using what is known from the experimental data, T_i^j, we try to determine such values. We specify the parameter a_i's for which values are determined. Since many experimental data points T_i^j are given, we commonly use the least–squares method, as follows:

Find the parameters $A = [a_0, a_1, a_2, a_3]$ that minimize the functional

$$F(A) = \sum_i \sum_j \left[T_i^j - T_e(x_i, t^j) \right]^2 \tag{20}$$

where the $T_e(x_i, t^j)$ is the experimental data at time t^j at the location x_i, and w_i^j is the value of the computed solution $w(x,t)$ for the non–linear diffusion at time $t=t^j$ at the location $x=x_i$ by the finite volume method explained in the preceding clause.

The necessary condition under which the functional is minimized at the A^* is

$$\nabla F(A^*) = 0 \tag{21}$$

Then the gradient of $F(A)$ is

$$\nabla F(A) = \sum_{i=1}^{m} r_i(A) \nabla r_i(A) = J(A)^T r(A) \tag{22}$$

where $r(A) = (r_1, r_2, \cdots r_m)^T$, $r_i(A) = T_i^j - T_e(x_i, t^j)$, and the Jacobian matrix of $r(A)$ is

$$J(A) = \begin{pmatrix} \frac{\partial r_1}{\partial a_0} & \frac{\partial r_1}{\partial a_1} & \frac{\partial r_1}{\partial a_2} & \frac{\partial r_1}{\partial a_3} \\ \frac{\partial r_2}{\partial a_0} & \frac{\partial r_2}{\partial a_1} & \frac{\partial r_2}{\partial a_2} & \frac{\partial r_2}{\partial a_3} \\ \vdots & \vdots & \vdots & \vdots \\ \frac{\partial r_m}{\partial a_0} & \frac{\partial r_m}{\partial a_1} & \frac{\partial r_m}{\partial a_2} & \frac{\partial r_m}{\partial a_3} \end{pmatrix} \tag{23}$$

However, this system of equations is difficult to compute and is nonlinear. Hence, Newton's method is used to solve this system. The original Newton's iterative formula has the form.

$$A^{(k+1)} = A^{(k)} - [J(A^{(k)})^T J(A^{(k)}) + S(A^{(k)})^{-1} J(A^{(k)})^T r(A^{(k)}) \tag{24}$$

where Hessian $S(A)$ has the second–order derivative, such as

$$S(A) = \sum_{i=1} r_i(x) \nabla^2 r_i(x) \tag{25}$$

However, $S(A)$ is expensive to compute and makes the system ill–conditioned. Hence, by neglecting this second–order term in Newton's method, the simplified iteration is as follows:

$$A^{(k+1)} = A^{(k)} - [J(A^{(k)})^T J(A^{(k)})]^{-1} J(A^{(k)})^T r(A^{(k)}) \tag{26}$$

This equation is said to be the Gauss–Newton iteration. To make the iteration well–defined, it is required that the rank of the Jacobian matrix be 4. Obviously, the success of the Gauss–Newton method will depend on the importance of the neglected second–order term $S(A)$. If $S(A^*)=0$, then the Gauss–Newton method would have a quadratic convergence rate.

RESULTS AND DISCUSSION

Experimental results

To minimize estimation error of the sky temperature, it is desirable for the experiments to be conducted on a clear day. Our two field tests, therefore, could not be conducted consecutively. The cloud cover index at three–hour intervals is available from the local meteorological station. Adapting them to the simulation, however, did not give better results, and the cloudiness was not considered in this study. Therefore, we acknowledge that some errors are possible in our estimated results.

On April 30th, the weather was mostly sunny, as shown in Figure 2, and the maximum solar radiation was 891 W/m^2. On June 5th, the weather was cloudier, and the maximum solar radiation was 996 W/m^2. The air temperature and relative humidity were higher than those on April 30th. On both days, the wind speed was rather

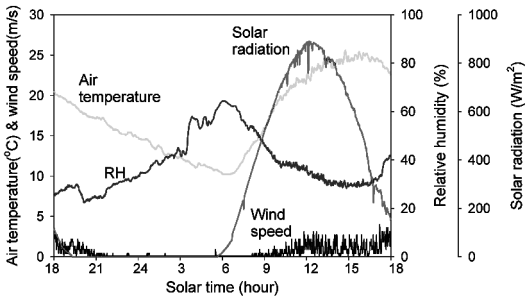

(a) April 30, 2009

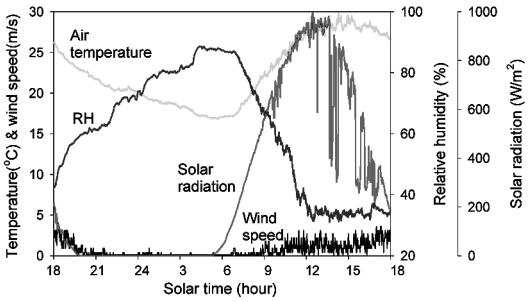

(b) June 5, 2009

Fig. 2. Weather data as measured at Gwangju, Korea.

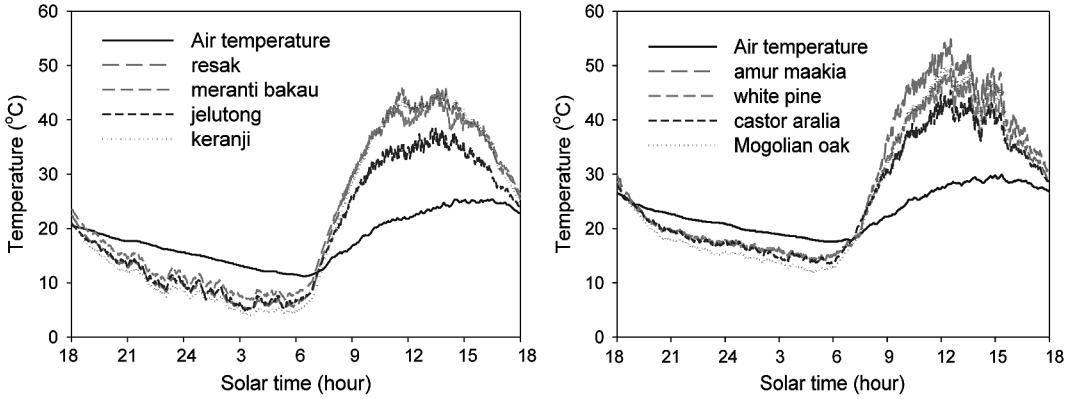

Fig. 3. Measured surface temperature of tropical hardwoods and Korean wood.

low, 0.1 m/s to 5.0 m/s, and there was especially little wind at midnight. The average wind speed on April 30th and June 5th was 0.6 m/s and 1.2 m/s, respectively. The sky temperature depends on the dew point and increases with decreases in the relative humidity (Eqs. 10 and 11). Even though the air temperature was the same on both days, therefore, the sky temperature on April 30th was higher than on June 5th.

Figure 3 shows the surface temperature of tropical hardwood and Korean wood. Exposed to the outdoor environment, the surface temperature is not in a state of equilibrium with the air temperature but, instead, is in a dynamic state that is always below or above the air temperature. The highest nocturnal surface temperatures were attained by Amur maakia, a Korean wood, and resak, a tropical hardwood. The nocturnal surface temperatures of the Mongolian oak, a Korean wood, and keranji, a tropical hardwood, were the lowest. The maximum surface temperature of tropical hardwood and Korean wood was 14.9~24.1 ˚C and 17.4~26.7 ˚C higher than the air temperature during the daytime, respectively. These differences in maximum temperature are mainly due to the amount of solar radiation present on the experimental days. During the night, however, the surface temperature of the wood was 6.1~8.8 ˚C and 3.9~6.1 ˚C colder than the outdoor air as a result of radiation to the sky, respectively.

It should be noted that nocturnal surface temperature can be much lower than the minimum temperature investigated in this study in cases where there is a lower sky temperature (lower relative humidity, clearer sky) and a higher wind speed.

Estimation of solar absorptivity and emissivity

Typical comparisons between measured and estimated surface temperatures are shown in Figure 4. Amur maakia showed the largest discrepancy and costata birch the smallest among the Korean wood species. The error at night was lower than that during daylight. The average absolute error was 0.63 ˚C (0.50~0.97 ˚C) for Korean wood and was 0.86 ˚C (0.64~1.47 ˚C) for tropical hardwood. Such errors could be due to measurement errors during installation causing, for example, thermal contact resistance between wooden surfaces and thermocouples.

Emissivity is involved in the calculation throughout the day and night, but absorptivity is a factor only during daylight hours. Because the calculation time was equally weighted in the process of the least squares method, the estimation of emissivity is more dominant than that of absorptivity. In all wooden specimens, there was a lower error at night, and the emissivity estimates were fairly accurate. However, there was a higher error during the day because both the absorptivity, as well as the emissivity, were involved in the calculation, and the absorptivity is likely to be calculated with a given emissivity. Therefore, the higher emissivity resulted in a higher absorptivity.

The simplified heat transfer equation, h=a+bV (V = wind velocity), was also evaluated, as it is frequently used in building physics. In the case of the ASHRAE (2001) heat transfer equation (a=5.8, b=3.7), the absorptivity was 89% lower, but the emissivity was 107% higher, than those of the results shown in Table 1. Thus, the heat transfer coefficient during the night was higher, but lower during the daytime, than the dimensionless heat transfer equation adapted in this study. The absolute error increased, especially in the case of the tropical hardwoods, and the results gave lower correlations with color. The convective heat transfer coefficients assumed had a great effect on the absorptivity and emissivity estimated by the inverse method. As the coefficients increased, higher absorptivity and emissivity resulted.

In general, the absorptivity and emissivity depend on surface material finish, surface temperature, and the wavelength and direction of the incident radiation. The absorptivity and emissivity of wood obtained by the inverse method are shown in Tables 1 and 2. The average absorptivity and emissivity investigated in this study were 0.396 (0.308~0.570) and 0.526 (0.307~0.772), respectively. In general, the absorptivity of nonconductors, such as wood, is lower than the emissivity. For some species, however, the absorptivity was greater than the emissivity, especially with meranti bakau. The ratio of absorptivity to emissivity ranged from 0.542 to 1.334, with an average of 0.748. It is known that the emissivity of most nonmetals is above 0.8 and much higher than

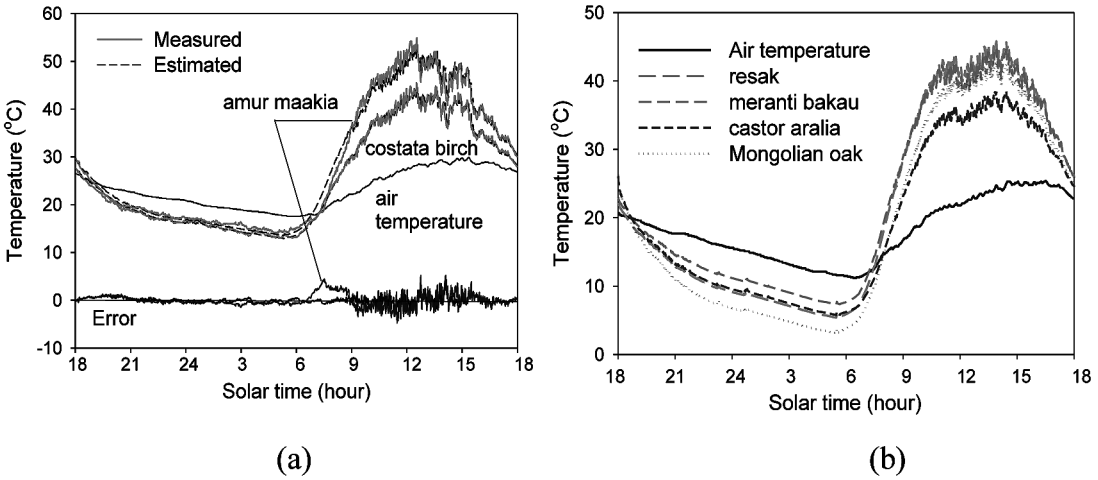

Fig. 4. Simulation results (a) Comparison between measured and estimated surface temperatures (b) Maximum and minimum surface temperatures by simulation.

those of metals (McAdams, 1954). The emissivity of wood is assumed to be about 0.9, as represented in most textbooks. However, the emissivity estimated in this study was much lower for most species than the values found in previous studies.

Peak wood surface temperature is generally affected by solar absorptivity during the day under the same outdoor environment, while it is affected by emissivity during the night. However, it should be noted that simply decreasing the absorptivity of a material's surface may not be effective in reducing its temperature and heat gain if its emissivity is reduced simultaneously (Simpson JR and McPherson EG, 1997).

To investigate the daily thermal variations of wood, the daily temperature changes of Korean wood, with absorptivity and emissivity obtained by the inverse method (Table 1), were calculated at a given weather condition, April 30th. Figure 4(b) shows the resulting maximum and minimum surface temperature variations of wood investigated in this study.

Wood color and absorptivity

CIELAB color system, L* a* b*, is an approximately uniform color space in rectangular coordinates based on a nonlinear expansion of the tristimulus values and taking the differences to produce three opponent axes that approximate the percepts of darkness– lightness, greenness–redness, and blueness–yellowness (ASTM D 2244–07, 2007). As Nishino *et al.* (1998) reported, the values vary widely among wood species (Table 1 and 2).

The relationship between the colorimetric values (L*a*b*) and the density, which ranges from 336 kg/m^3 to 1181 kg/m^3, is as shown in Figure 5(a). Negative correlations were found for the values L* and b* versus the density, while a positive relationship was found between the value of a* and the density. R^2 of the L*, a*, and b* versus the density were 0.356, 0.122, 0.242, respectively. Lightness or whiteness has the highest correlation with density. As shown in Figure 5(b), the correlation between density and absorptivity was 0.444 due to the relationship between the color and the density. Absorptivity tends to increase with increasing density.

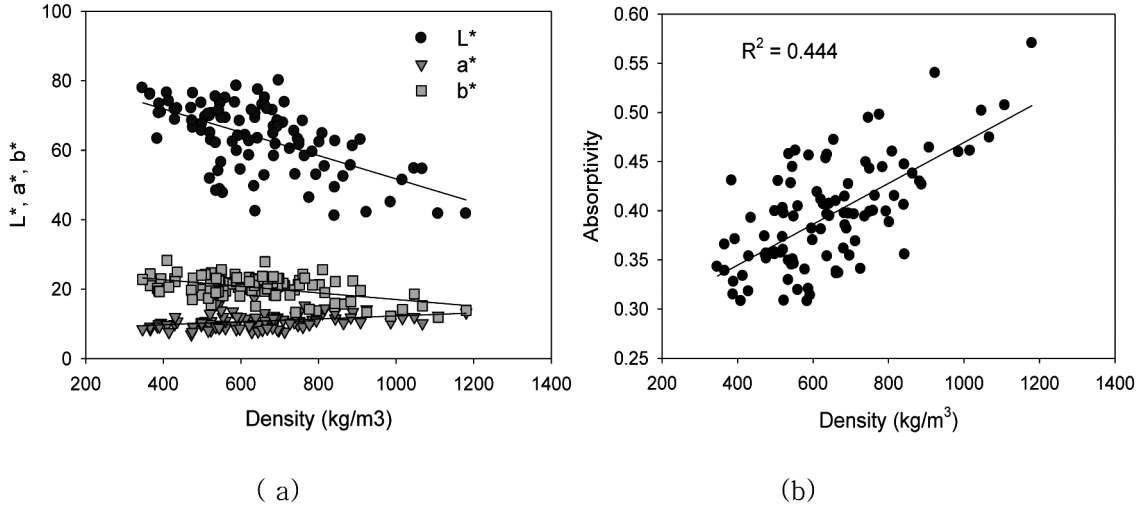

Fig. 5. Relation of density with color and absorptivity.

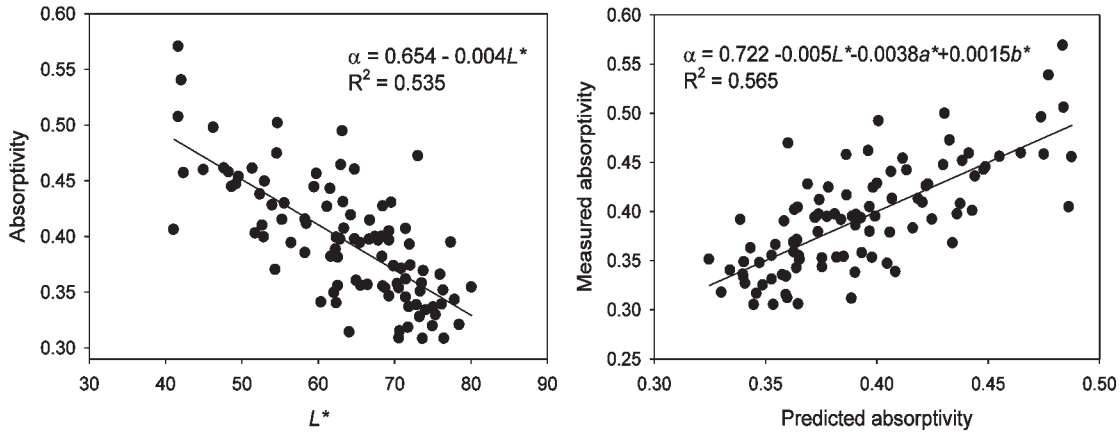

Fig. 6. Colors and absorptivity.

Figure 6(a) shows that the absorptivity decreases with increases in the value of L*. Furthermore, the correlation coefficient between the color system and the absorptivity increased slightly by multiple regression, as shown in Figure 6(b). From these results, the color of wood exposed to sunlight was expected to influence the thermal performance of wood components significantly, as the color determines the amount of absorbed solar radiation. Applying a light colored wood is, indeed, the simplest, most effective, and most economical means to reduce indoor temperature in hot–humid climates. However, it should be noted that the color of a surface may not indicate its overall capacity as an absorber or reflector, since much of the irradiation may be in the infrared (IR) region (Incropera *et al*., 2007).

It is known that the emissivity of metals depends strongly on the nature of the surface material, which can be influenced by the method of fabrication, thermal cycling, and chemical reactions with its environment (McAdams WH, 1954). However, there was not any relationship between emissivity and color or density. There was a weak positive correlation between absorptivity and emissivity overall with R2=0.223. Grouping results by experimental days revealed a higher correlation between them (Figure 7). However, this may or may not be due to material characteristics or the limitations of numerical analysis, including the assumed equations and inverse method.

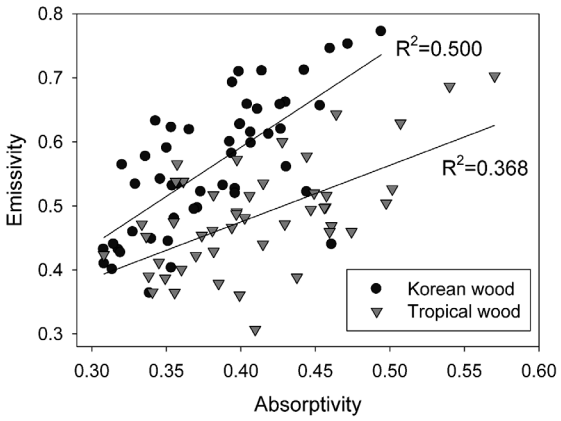

Fig. 7. Relation of absorptivity with emissivity.

CONCLUSION

By using experimental field measurements of wood surface temperature, the solar absorptivity and emissivity of various wood species were estimated using the inverse method. Absorptivity ranged from 0.308 to 0.526. Estimated emissivity ranged from 0.307 to 0.772, with values much lower than those found in most previous studies. Our results can guide future studies in predicting the thermal performance of wood exposed to outdoor conditions, at least as a first approximation.

Lightness decreased with density while absorptivity increased with density. Absorptivity was closely related to the color system, especially to whiteness. It decreased with increasing values of whiteness or L*, which is consistent with previous results. However, there was not any relationship between emissivity and color or density.

Thermocouples inevitably change the local characteristics, such as the absorptivity, emissivity, and conductivity. Installation errors are also caused by thermal contact resistance between wooden surfaces and thermocouples. Furthermore, heat radiation with surrounding objects might produce some errors, and this was not considered in this study. Solar absorptivity and emissivity obtained by the inverse method were highly dependent on the assumed external heat transfer coefficients. Therefore, the absorptivity and emissivity obtained in this study might be less precise than desired. Further systematic study would be necessary to directly measure these parameters.

ACKOWLEDGEMENT

This work was supported by a Korean Research Foundation Grant, funded by the Korean Government (MOEHRD) (The Regional Research Universities Program/Biohousing Research Institute), Basic Research

Program through the National Research Foundation of Korea(NRF) funded by the Ministry of Education, Science and Technology(No. 2009–0075067), and the Brain Korea 21 Program, funded by the Ministry of Education, Republic of Korea.

REFERENCES

ASHRAE 2001 *ASHRAE Fundamentals Handbook*. American Society of Heating, Refrigerating and Air conditioning Engineers. Atlanta, GA

ASTM D 2244–07, 2007 Standard practice for calculation of color tolerances and color differences from instrumentally measured color coordinates

Berdahl, P. and M. Martin 1984 Emissivity of clear skies. Technical Note. *Solar Energy*, **32**(5): 663–664

Bansal, NK., SN. Garg and S. Kothari 1992 Effect of exterior surface colour on the thermal performance of buildings. *Building and Environment*, **27**(1): 31–37

Cole, RJ. 1976a The longwave radiation incident upon the external surface of buildings. *The Building Service Engineer*, **44**: 195–206

Cole, RJ. 1976b The longwave radiative environment around buildings. *Building and Environment*, **4**: 1–13

Cole, RJ. 1979 The longwave radiation incident upon inclined surfaces. *Solar Energy*, **11**: 459–462

Duffie, JA, and WA. Beckman 1991 *Solar Engineering of Thermal Processes*. 2nd Ed. John Wiley & Sons Inc. New York. USA

FPL Wood Handbook 1999 wood as an engineering material. Madison, WI : USDA Forest Service, Forest Products Laboratory. General technical report FPL GTR–113

Heyer, OC. 1963 Study of temperature in wood parts of houses throughout the United States. US Forest Service RN FPL–012, Madison, Wis

Incropera, FP., DP. Dewit, TL. Bergman and AS. Lavine 2007 *Fundamentals of heat and mass transfer*. 6th Ed. John Wiley & Sons

Kragh, MK. 1998 Microclimatic conditions at the external surface on building envelopes. Report R–027. Dept of Buildings and Energy, Technical Univ of Denmark

McAdams, WH. 1954 *Heat Transmission*. 3rd ed., McGraw–Hill, New York

Nishino, Y., G. Janin, B. Chanson, Detienne, J. Gril and B. Thibaut 1998 Colorimetry of wood specimens from French Guiana. *J Wood Sci*, **44**: 3–8

Simpson, JR. and EG McPherson 1997 The effects of roof albedo modification on cooling loads of scale model residence in Tucson Arizona. *Energy and Buildings*, **25**: 127–137

Shida, S., M. Satoh and T. Arima 1991 Utilization and evaluation of exterior wood I : relationships between meteorological elements and surface temperatures of wood deck. *Mokuzai Gakkaishi*, **37**(12): 1188–1192

Tenwolde, A. 1997 FPL roof temperature and moisture model : Description and verification. FPL–RP–561. Madison, WI: US Department of Agriculture, Forest Service, Forest Products Laboratory

Wengert, EM. 1965 Predicting maximum surface temperatures of wood in exterior exposures. *Forest Prod J*, **15**(7): 263–268

Wilkes, KE. 1989 Model for roof thermal performance. ORNL/CON–274. Oak Ridge, TN: Oak Ridge National Laboratory